# Characterizing the regimes of spray flame-vortex interactions: A spray spectral diagram for extinction

**By B. Franzelli, A. Vié AND M. Ihme**

## 1. Motivation and objectives

The flame-vortex interaction is a canonical configuration for theoretical understanding of the combustion mechanisms in turbulent flows (Poinsot *et al.* 1991). Specifically, under the flamelet hypothesis, the turbulent flame front is seen as a collection of one-dimensional flames that are stretched and deformed by vortices (Peters 1984). Indeed, the effect of a pair of vortices on a laminar flame can be studied to characterize numerous combustion regimes occurring in a turbulent flow (Poinsot & Veynante 2012). Even if the flame-vortex interaction is recognized as an intermediate academic configuration, representative of the interaction of combustion with turbulence, theoretical and experimental investigations remain limited (Shiah & Sichel 1993; Santoro *et al.* 2000; Santoro & Gomez 2002; Lemaire *et al.* 2002, 2005). In particular, the interaction of a pair of vortices with a spray flame is examined to identify the effect of the evaporation process on combustion regimes for turbulent spray flames. The specific focus here is on the characterization of local extinction and the derivation of a spectral diagram for spray flames from analytic arguments. The validity of the spectral diagram is subsequently verified using details numerical simulations.

## 2. Background: Gaseous flame-vortex interaction

The flame-vortex interaction is an academic configuration, enabling the study of basic phenomena that control the coupling between combustion and turbulence. Using such a configuration, Renard *et al.* (2000) give a fundamental understanding of different combustion modes, which are summarized in the so-called spectral diagram. In the following, we briefly summarize the classical results for gaseous flames.

The configuration consists of a strained non-premixed flame, in which a mixture of fuel diluted with nitrogen is injected against an oxidizer stream (cf. Figure 1). A vortex ring of radius $r_0$ and strength $\Gamma$ is injected on the oxidizer side to interact with a flame front. Due to the vortex interaction, the flame, which is subjected to a strain rate $A_0$ for the unperturbated flow, will experience a strain $A_\Gamma = \Gamma/(2r_0^2)$. Eventually, the flame can locally extinguish when $A_\Gamma$ exceeds the critical extinction strain rate $A_e$. Depending on the non-dimensional vortex strength ($\widetilde{\Gamma} = A_\Gamma/A_0$), the robustness of the flame ($R = A_e/A_0$), and the Peclet number of the unperturbed flow ( $\mathrm{Pe}_0 = A_0 r_0^2/D_T$, where $D_T$ is the thermal diffusivity†), different regimes can be identified (Vera *et al.* 2007): (i) vortex dissipation ($\mathrm{Pe}_0\widetilde{\Gamma} < 1$), as for small vortex strength, the vortex dissipates before reaching the flame front without affecting the flame; (ii) thickened reaction zone ($(\mathrm{Pe}_0 R)^{1/2} < 1$),

† The Peclet number could equivalently be defined as $\mathrm{Pe}_0 = A_0 r_0^2/\nu$, where $\nu$ is the kinematic viscosity of the oxidizer stream.

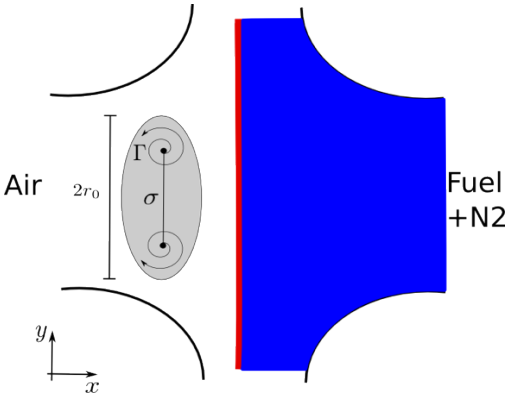


FIGURE 1. Schematic of the gaseous configuration: two counter-rotative vortices are superimposed to the initial steady state solution of the counterflow flame without spray injection on the fuel side.

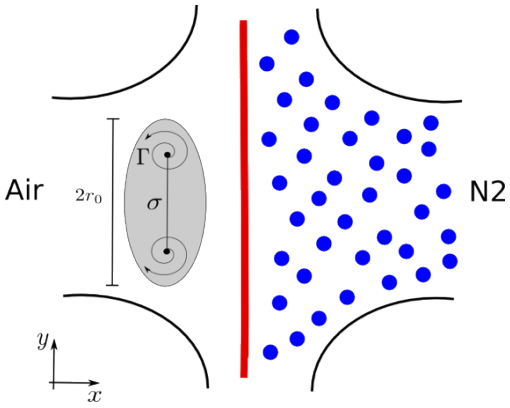


FIGURE 2. Schematic of the spray configuration: two counter-rotative vortices are superimposed to the initial steady state solution of the counterflow flame with spray injection on the fuel side.

[p]

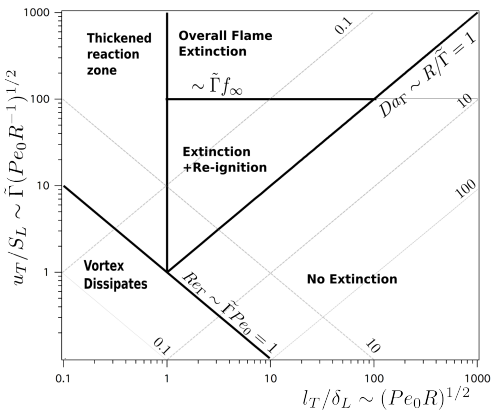


FIGURE 3. Spectral diagram for purely gaseous flame-vortex interaction.

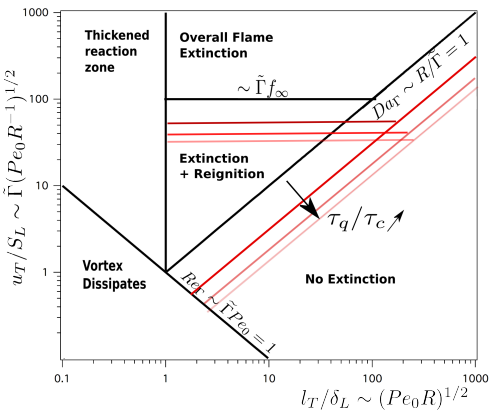


FIGURE 4. Spectral diagram for spray flame-vortex interaction.

for which a thickening of the reaction zone may occur without relevant modification of the flame structure, as the vortex size is smaller than the laminar flame thickness; (iii) local flame extinction ($R/\widetilde{\Gamma} < 1$ ), for which if the vortex is sufficiently strong and large to extinguish the flame; (iv) flame re-ignition via edge flame ($(\mathrm{Pe}_0 R^{-1})^{1/2} < f_\infty$, with $f_\infty \approx 3$ (Vera *et al.* 2007), for which, in the case of local extinction, the flame front could re-ignite if the flame-front velocity $U_F$ is of the same order as the flow velocity.

Such regimes are classically represented in the spectral diagram represented in Figure 3. The flame-vortex interactions are here represented as a function of the non-dimensional size and velocity of the vortex, where $\delta_L$ is the thickness of the diffusion flame, and the characteristic speed $S_L = \delta_L/\tau_c$ is obtained from the chemical time scale $\tau_c$; $u_T \sim \Gamma/r_0$ and $l_T \sim r_0$ are the characteristic speed and size of the vortex. Turbulent vortices and unsteady chemistry effects could also be taken into account (Vera *et al.* 2007).

## 3. Spectral diagram for spray flame-vortex interaction

The spectral diagram is here extended to consider the interaction of a pair of vortices with a spray flame. On the fuel side, a fuel spray is injected together with gaseous nitrogen against a stream of oxidizer. Spray is expected to have a compounding effect on the flame-vortex interaction, due to the introduction of two additional characteristic time scales: the evaporation time $\tau_v$ and the droplet drag time $\tau_p$. In this asymptotic analysis, both $\tau_v$ and $\tau_p$ are assumed to be constant. A relation for this time-scale ratio can be expressed as (Réveillon & Vervisch 2005)

$$\frac{\tau_p}{\tau_v} = \frac{4}{9}\frac{ln(1+B_M)}{\mathrm{Sc}} = \frac{\mathrm{St}}{\mathrm{St}_v} = \text{constant} = \kappa, \tag{3.1}$$

where $B_M$ is the Spalding number , Sc is the Schmidt number of the gas phase, $\mathrm{St} = \tau_p A_0$ is the drag Stokes number, and $\mathrm{St}_v = \tau_v A_0$ is the evaporation Stokes number. These two additional characteristic time scales affect both the flow and the flame quantities, compared to the corresponding gaseous flame.

For the vaporization time $\tau_v$, the main contribution is assumed to be the change of the characteristic quenching time $\tau_q$ of the flame and, consequently, the flame properties

$$S_L \rightsquigarrow S_L^* = S_L^*(S_L, \tau_v) = S_L^*(\tau_c, \tau_v), \tag{3.2a}$$

$$\delta_L \rightsquigarrow \delta_L^* = \delta_L^*(\delta_L, \tau_v) = \delta_L^*(\tau_c, \tau_v), \tag{3.2b}$$

$$A_e \rightsquigarrow A_e^* = A_e^*(A_e, \tau_v) = A_e^*(\tau_c, \tau_v), \tag{3.2c}$$

$$U_F \rightsquigarrow U_F^* = U_F^*(U_F, \tau_v) = U_F^*(\tau_c, \tau_v), \tag{3.2d}$$

where the superscript $^*$ indicates that the quantity is modified by the evaporation time.

Considering the drag time $\tau_p$, the main effect is a velocity difference between gas and liquid phases for large Stokes numbers ($\tau_p \gg A_0^{-1}$). For a two-way coupling, the spray can locally modify the strain rate of the unpertubated flow but not the vortex properties (since it is injected on the oxidizer side):

$$A_0 \rightsquigarrow A_0^\ddagger = A_0^\ddagger(A_0, \tau_p), \tag{3.3}$$

where the superscript $\ddagger$ indicates that the quantity is modified by the drag time. Moreover segregation could cause some mixture-fraction inhomogeneities, affecting the spray flame properties $S_L^*, \delta_L^*, A_e^*$:

$$S_L^* \rightsquigarrow S_L^\ddagger = S_L^\ddagger(S_L^*, \kappa) = S_L^\ddagger(\tau_c, \tau_v, \kappa), \tag{3.4a}$$

$$\delta_L^* \rightsquigarrow \delta_L^\ddagger = \delta_L^\ddagger(\delta_L^*, \tau_v, \kappa) = \delta_L^\ddagger(\tau_c, \tau_v, \kappa), \tag{3.4b}$$

$$A_e^* \rightsquigarrow A_e^\ddagger = A_e^\ddagger(A_e^*, \tau_v, \kappa) = A_e^\ddagger(\tau_c, \tau_v, \kappa), \tag{3.4c}$$

$$U_F^* \rightsquigarrow U_F^\ddagger = U_F^\ddagger(U_F^*, \tau_v, \kappa) = U_F^\ddagger(\tau_c, \tau_v, \kappa). \tag{3.4d}$$

With this, the different flames/vortex interactions can be extended to spray flames. The first regime is the vortex dissipation for which the vortex strength is too small so that it dissipates before reaching the flame

$$\mathrm{Re} = \frac{\Gamma}{\nu} = \frac{\Gamma}{2(r_0)^2 A_0^\ddagger}\frac{2(r_0)^2 A_0^\ddagger}{\nu} \sim \tilde{\Gamma}^\ddagger \mathrm{Pe}_0^\ddagger \leq 1. \tag{3.5}$$

When the vortex is strong enough but small compared to the flame thickness, a thickened

reaction zone regime occurs: the vortex penetrates the preheat flame region and enhances the mixing of the reactants. The flame then presents a thickened preheat zone, but its inner structure is not affected by the vortex

$$\frac{l_T}{\delta_L^\ddagger} \sim \left(\mathrm{Pe}_0^\ddagger R^\ddagger\right)^{1/2} \leq 1; \tag{3.6}$$

For a flame strength $R^\ddagger$ smaller than the non-dimensionalized vortex strength $\tilde{\Gamma}^\ddagger$, the vortex pair extinguishes the flame, and a local flame extinction regime is observed

$$R^\ddagger = \frac{A_e^\ddagger}{A_0^\ddagger} \leq \frac{A_\Gamma^\ddagger}{A_0^\ddagger} = \tilde{\Gamma}^\ddagger \Rightarrow \mathrm{Da}_\Gamma^{\ddagger,e} = \frac{A_e^\ddagger}{A_\Gamma^\ddagger} \sim \frac{R^\ddagger}{\tilde{\Gamma}^\ddagger} \leq 1, \tag{3.7}$$

where $\mathrm{Da}_\Gamma^{\ddagger,e}$ is the Damköhler number at extinction. Once extinction has occurred, the two separate flame fronts may reignite whenever the propagation velocity $U_F^\ddagger$ is higher than the characteristic strain-rate induced velocity $A_0^\ddagger r_0^\ddagger$, in the so-called flame reignition via edge flame regime

$$\frac{U_F^\ddagger}{S_L^\ddagger} \geq \frac{A_0^\ddagger r_0}{S_L^\ddagger} \sim \left(\frac{\mathrm{Pe}^{\ddagger_0}}{R^\ddagger}\right)^{1/2}. \tag{3.8}$$

According to Hermanns *et al.* (2007) and Fernandez-Tarrazo *et al.* (2006), the front velocity $U_F$ of a purely gaseous triple flame reaches values of order $S_L f_\infty$. In analogy, this relation is also assumed for spray flames

$$\frac{U_F^\ddagger}{S_L^\ddagger}\frac{1}{f_\infty^\ddagger} \sim 1, \tag{3.9}$$

obtaining the condition for reignition

$$(\mathrm{Pe}_0^\ddagger {R^\ddagger}^{-1})^{1/2} \leq f_\infty^\ddagger. \tag{3.10}$$

Compared to the gaseous spectral diagram for which the value of $f_\infty$ has been evaluated from triple flames, an estimation for $f_\infty^\ddagger$ has still to be provided for spray flames and is not a part of the present work.

## 4. Analytical spray spectral diagram based on the evaporation time

To simplify the problem, a dilute regime is assumed here, i.e., a one-way coupling exists between the gaseous and the liquid phases. This assumption is reasonable when considering that droplets follow the mean flow, i.e., $\mathrm{St} = \tau_p A_0 \ll 1 \Rightarrow \kappa << (A_0\tau_v)^{-1}$, and droplets also follow the vortex, i.e., $\tau_p A_\Gamma <\ll 1 \Rightarrow \kappa << (A_\Gamma \tau_v)^{-1}$.

Then, the only role of the evaporation process is evaluated by considering a constant evaporation time $\tau_v$. The effect of evaporation is accounted for in the spectral diagram by assuming that its main contribution is the change in the characteristic quenching time $\tau_q$ of the flame (Ballal & Lefebvre 1981)

$$\tau_q = \tau_v + \tau_c. \tag{4.1}$$

The evaporation time does not affect the diffusion flame thickness, and the other flame properties could be derived from the purely gaseous values

$$\frac{\delta_L^*}{\delta_L} \sim 1, \tag{4.2a}$$

$$\frac{S_L}{S_L^*} \sim \frac{\tau_q}{\tau_c}, \tag{4.2b}$$

$$\frac{\mathrm{Da}_\Gamma^e}{\mathrm{Da}_\Gamma^{*,e}} \sim \frac{A_e}{A_e^*} \sim \frac{\tau_q}{\tau_c}. \tag{4.2c}$$

These relations are supported by experimental and numerical data for stoichiometric premixed spray flames (Ballal & Lefebvre 1981; Senoner 2010). The Damköhler number at extinction strain rate is smaller for high values of the evaporation time, implying that a spray flame extinguishes for smaller values of the strain rate than that of a gaseous flame, as found by Dvorjetski & Greenberg (2002). In Hermanns *et al.* (2007), the front propagation velocity $U_F^*$ for purely gaseous flames is observed to be a function of the Damköhler number, which presents an asympotic value. This behavior is here also assumed for spray flames

$$\frac{U_F}{S_L}\frac{1}{f_\infty} = f(\mathrm{Da}/\mathrm{Da}^e) \sim 1 \Rightarrow \frac{U_F^*}{S_L^*}\frac{1}{f_\infty^*} = f(\mathrm{Da}^*/\mathrm{Da}^{*,e}) \sim 1. \tag{4.3}$$

Then, the classical asymptotic analysis, discussed by Thevenin *et al.* (1998) for gaseous flame-vortex interactions, is extended to spray flames using the relation between gaseous and spray flame properties. Compared to the regime diagram for gaseous flames, an additional third dimension, i.e., the non-dimensional quenching time $\tau_q/\tau_c$, has to be considered. This time scale does indeed changes the way the vortex interacts with the flame, by changing the characteristics flame properties. This is clearly identified in the spectral diagram represented in Figure 4. Here, the black lines limit the different combustion modes that were analytically found for gaseous flames, and the red lines correspond to spray flames with increasingly higher evaporation time. By considering only the effect of the evaporation time on the criteria given in Section 3, it is possible to define the limits of the spectral diagram. The vortex dissipation region ($\mathrm{Re} \leq 1$) is identified by a diagonal line with a slope of $n = -1$ in the $u_T/S_L$-$l_T/\delta_L$ log-log diagram:

$$\frac{u_T}{S_L}\frac{l_T}{\delta_L} \leq 1. \tag{4.4}$$

As expected, this area is unchanged compared to that of purely gaseous combustion since the spray is assumed not to affect the flow-field properties. The thickened reaction zone ($l_T/\delta_L \sim 1$) is identified by a vertical line in the $u_T/S_L$-$l_T/\delta_L$ diagram

$$\frac{l_T}{\delta_L} \leq 1. \tag{4.5}$$

Since the flame thickness of the diffusion flame is not affected by the evaporation time, this region is unchanged compared to that in gaseous flames. The local extinction region ($\mathrm{Da}_\Gamma^{*,e} \leq 1$) is represented by the diagonal with a unity slope in the $u_T/S_L$-$l_T/\delta_L$ diagram

$$\frac{u_T}{S_L}\frac{\delta_L}{l_T} \sim \frac{1}{\mathrm{Da}_\Gamma^e} \leq \frac{\tau_c}{\tau_q} \Rightarrow \frac{u_T}{S_L}\frac{\delta_L}{l_T}\frac{\tau_q}{\tau_c} \leq 1. \tag{4.6}$$

Then, the extinction area increases for longer evaporation times, i.e., local extinction occurs for smaller values of the vortex strain rate. Finally, the reignition condition ($U_f^*/S_L^* \leq f_\infty^*$) is verified for the region identified by the -1/2 slope in the $u_T/S_L$-$\tau_q/\tau_c$ diagram

$$\frac{u_T}{S_L} \leq \tilde{\Gamma} f_\infty^* \left(\frac{\mathrm{Da}_\Gamma^{*,e}}{\mathrm{Da}_\Gamma^e}\right)^{1/2} \leq \tilde{\Gamma} f_\infty^* \left(\frac{\tau_q}{\tau_c}\right)^{-1/2}, \tag{4.7}$$

using the relation $U_T/S_L \sim \widetilde{\Gamma}(\mathrm{Pe}/R)^{1/2}$. The reignition area decreases with evaporation time, showing that for large droplet diameters the flame is more likely to extinguish than for a purely gaseous flame. The value for $f^*_\infty$ may be assumed to be of the order of unity, in analogy with gaseous flames.

In the following, this spectral diagram is verified through numerical simulations. Note that a complete characterization of the reignition phenomenon will require an extensive study on edge spray flames, which is beyond the scope for this work. In addition, we will focus on the extinction phenomena without investigating the reignition stage of our simulations.

## 5. Modeling and numerics

### 5.1. *Gas-phase equations*

The gas phase is described by the conservation equations for mass, momentum, species, and energy

$$\mathrm{D}_t\rho = \dot{S}_m, \tag{5.1a}$$

$$\mathrm{D}_t(\rho u_i) = \dot{S}_{u_i} - \partial_i p + \partial_j(\sigma_{ij}) \ , \tag{5.1b}$$

$$\mathrm{D}_t(\rho Y_k) = \partial_j\left(\rho D_k \frac{W_k}{W}\partial_j X_k\right) + \dot{\omega}_k + \dot{S}_m\delta_{kF} \ , \tag{5.1c}$$

$$\mathrm{D}_t(\rho T) = \partial_j\left(\frac{\lambda}{c_p}\partial_j T\right) + \frac{\lambda}{c_p^2}\partial_j T\partial_j c_p - \sum_{k=1}^{N_s}\frac{h_k\dot{\omega}_k}{c_p} + \dot{S}_T \ , \tag{5.1d}$$

where $\mathrm{D}_t\phi = \partial_t\phi + \partial_i u_i\phi$, $\partial_i \equiv \partial_{x_i}$; $\rho$ is the gas density; $u_i$ is the gas velocity; $\dot{S}_m$, $\dot{S}_{u_i}$, and $\dot{S}_T$ are the source terms due to droplet evaporation, drag force, and heat transfer, respectively. The mass fraction and mole fraction of species $k$ are denoted by $Y_k$ and $X_k$, respectively. The pressure is denoted by $p$, and $\sigma_{ij} = \mu\left[\partial_i u_j + \partial_j u_i - \frac{2}{3}\partial_k u_k\delta_{ij}\right]$ is the viscous stress tensor. The molecular weight of species $k$ is denoted by $W_k$, and $W$ is the mixture-averaged molecular weight. The diffusivity of species $k$ is denoted by $D_k$, $\dot{\omega}_k$ is the reaction source term of species $k$, and $\delta_{kF}$ is the Kronecker function that is unity for fuel and zero for all other species. The temperature is denoted by $T$, $\lambda$ is the thermal conductivity, $c_p$ is the heat capacity, and $h_k$ is the enthalpy of species $k$.

### 5.2. *Dispersed-phase equations*

For the dispersed phase, a Lagrangian point-particle approach is used (see Miller & Bellan 1999 for details). The equations describing each droplet are written as

$$\mathrm{d}_t x_{d,i} = u_{d,i}, \tag{5.2a}$$

$$\mathrm{d}_t u_{d,i} = f_{d,i} = \frac{f_1}{\tau_d}\left[u_i(\mathbf{x}_d) - u_{d,i}\right] \ , \tag{5.2b}$$

$$\mathrm{d}_t T_d = \dot{T}_d = \frac{\mathrm{Nu}}{3\mathrm{Pr}}\frac{c_p}{c_l}\frac{f_2}{\tau_d}\left[T(\mathbf{x}_d) - T_d\right] + \frac{\dot{m}_d l_v}{m_d c_l} \ , \tag{5.2c}$$

$$\mathrm{d}_t m_d = \dot{m}_d = -\frac{\mathrm{Sh}}{3\mathrm{Sc}}\frac{m_d}{\tau_d}\ln(1+B_M) \ , \tag{5.2d}$$

where $\boldsymbol{x}_d$ is the position of the droplet, $\boldsymbol{u}_d$ its velocity, $T_d$ its temperature, and $m_d$ its mass. Nu is the Nusselt number, Pr is the Prandtl number, Sh is the Sherwood number,

Sc is the Schmidt number, and $B_M$ is the Spalding number. The relaxation time of the droplet is $\tau_d = \rho_l d^2/18\mu$, $\rho_l$ is its density, $d$ is its diameter, $c_l$ is its heat capacity, and $l_v$ is the latent heat of vaporization. The drag factor is $f_1$, accounting for high Reynolds number effects, and $f_2$ is a correction factor to account for effects of heat exchange on the evaporation (Miller & Bellan 1999).

The coupling terms with the gas phase are obtained by integrating the contributions from all droplets contained in the control volume $\Delta V$:

$$\dot{S}_m = -\left\{\mathrm{d}_t m_d\right\}, \tag{5.3}$$

$$\dot{S}_{u_i} = -\left\{\mathrm{d}_t m_d u_{d,i}\right\}, \tag{5.4}$$

$$\dot{S}_T = -\frac{1}{c_p}\left\{c_l m_d \mathrm{d}_t T_d + (c_p T_d + l_v)\mathrm{d}_t m_d\right\}, \tag{5.5}$$

where $\{\cdot\} = \frac{1}{\Delta V}\sum_{d\in\Delta V}\cdot$.

To be consistent with the assumptions used to develop the analytical combustion diagram, the gas and spray phases are assumed at momentum equilibrium, i.e there is no slip velocity between both phases $u_{d,i} = u_i$. This assumption allows us to isolate the vaporization part of the spray physics, since the contribution of the drag force is zero. The heat transfer from liquid to gas is also assumed equal to zero, i.e., $\dot{S}_T = 0$.

### 5.3. *Reaction chemistry*

In the present study, a 24-species mechanism for n-dodecane is used (Vie *et al.* 2014), which is based on the JetSurF 1.0-l1 mechanism (Sirjean *et al.* 2009), originally consisting of 123 species and 977 reactions. The reduced mechanism has been validated in auto-ignition and perfectly stirred reactors (PSR) by Vie *et al.* (2014). Detailed thermodynamic and transport properties are considered. The species diffusivities $D_k$ are calculated assuming constant but not equal species Lewis number $\mathrm{Le}_k$, i.e., $D_k = \lambda\ (\rho c_p \mathrm{Le}_k)$.

### 5.4. *Numerics*

The governing equations are solved in the low Mach number limit using the structured 3DA code (Shashank 2012). A QUICK scheme is used for the discretization of the scalar advection operators, and a second-order central scheme is used for solving the momentum and pressure equations.The Poisson system is solved using the HYPRE library. A staggered representation is used where the velocity is defined at the cell face, while the scalars and density are located at the cell center. Time-integration is performed using a second-order Crank-Nicholson scheme. The chemical source terms are evaluated using the DVODE library, which uses an adaptive time stepping to advance the system of ODEs.

## 6. Setup of the configuration

We consider a two-dimensional counterflow configuration, consisting of two opposed slots. The direction $x_1 = x$ is the injection direction and the direction $x_2 = y$ is the outflow. The separation distance between the two injectors is $L_x = 0.1$ m, and $L_y = 0.075$ m is the vertical domain length. The mesh consists of $500 \times 370$ cells, guaranteeing at least 15 grid points to describe the diffusion flame (whose thickness is $\delta_L \approx 3$mm). At the fuel side, gaseous nitrogen is injected with a fuel spray composed of n-dodecane at ambient conditions ($T_d^F = T^F = 300$ K). Here and in the following, the superscripts F

and O refer to the fuel side and the oxidizer side, respectively. The liquid mass flow rate is 9 g/s, corresponding to a purely gaseous composition of $Y_{\mathrm{N_2}} = 0.68$ and $Y_{\mathrm{C_{12}H_{26}}} = 0.32$.

The initial droplet distribution at injection is randomly drawn over the entire slot, resulting in a statistically homogeneous distribution. A parcel method is used so that each numerical droplet statistically represents $N_p = 5$ physical droplets. On the oxidizer side, pure air is injected at $T^O = 800$ K. This operating condition ensures a robust flame with the liquid phase that mainly evaporates in the preheat zone. In the following, the injection velocity of the liquid phase is identical to that of the gas phase, $u^F = u^O = u_d^F = 2.5$ m/s, corresponding to a theoretical flame strain rate of $A_0 = 50\ \mathrm{s}^{-1}$.

Two counter-rotating vortices are superimposed on the steady-state velocity solution, on both sides of the symmetry axis $y = 0$. A schematic of the initialization procedure is presented in Figure 2. As suggested in Mantel *et al.* (1999), the Oseen vortex is used here. The equation of the velocity field in the vortex reference frame is

$$u_\theta = \frac{\Gamma}{2\pi r}\left(1 - \exp\left(-\frac{r^2}{r_v^2}\right)\right), \quad u_r = 0 \tag{6.1}$$

where $r = x/\cos(\theta)$, $\theta = \mathrm{atan}(\tilde{y}/\tilde{x})$, $\tilde{x} = x - x_v$, $\tilde{y} = y - y_v$, and $(x_v, y_v)$ is the initial position of the center of the vortex. $\Gamma$ is the vortex strength, and $r_v$ the initial vortex radius. The two vortices of equal radii and opposite strengths are initially separated by a distance $\sigma$, and they are at an equal distance $L_x$ from the symmetry axis $x = 0$. In the present study, the vortex is injected on the fuel side.

Following the recommendations of Mantel *et al.* (1999), the separation distance between the two vortices is set to $\sigma = 4r_v$, to avoid interactions between the viscous cores of the vortices.

To determine the characteristic length scale of the two vortices, the size of the perturbation in the $y$ direction is considered. As demonstrated in Mantel *et al.* (1999), the circulation induced by the Oseen vortex still exists until $3r_v$ away from the vortex center. Consequently, using the previous constraint on the vortex separation distance, the characteristic length scale of the perturbation is $l_T = 10r_v$.

## 7. Results and discussion

In Figures 5 and 6, the results of the simulations for different values of the circulation and the vortex radius are represented in the spectral diagram ($A_\Gamma$ = 250, 500, 1000, 2000, 3000, 5000, 10000 $\mathrm{s}^{-1}$ and $r_v = 1.5e^{-4}$, $6.0e^{-4}$, $1.5e^{-3}$, $3.0e^{-3}$ m). In order to map the spectral diagram, we perform simulations along isolines of characteristic strain rate $A_\Gamma$: first $A_\Gamma$ is fixed, then the radius of the vortex core is chosen, determining the value of the characteristic vortex velocity.

For the gaseous case, theoretically expected regions are retrieved, showing the relevance of the analytical study. For the spray case with negligible heating time, four scenarios are considered. (i) Vortex dissipation: the vortex is dissipated by viscous forces before reaching the flame front. Since the spray does not modify the flow field, this region is expected not to change, and the simulations confirm this statement. (ii) No extinction (case A, cf. Figure 7): below $R/\tilde{\Gamma} = \tau_q/\tau_c$, the interaction leads to a stretching of the flame that is not sufficiently strong to break the flame front. As expected by the analytical derivation, the limit is controlled by the quenching time and ,hence, the vaporization time of the droplets. (iii) Extinction due to strain rate (case B, cf. Figure 8): for conditions above $R/\tilde{\Gamma} = \tau_q/\tau_c$, the vortices are sufficiently strong to break the flame by stretching.

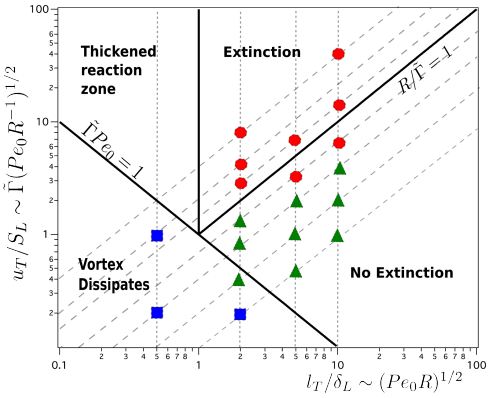


FIGURE 5. Spectral diagram for gaseous flame-vortex interaction: the symbols represent numerical simulations performed here. Squares represent the vortex dissipation regime, triangles the "no extinction", circles the local extinction.

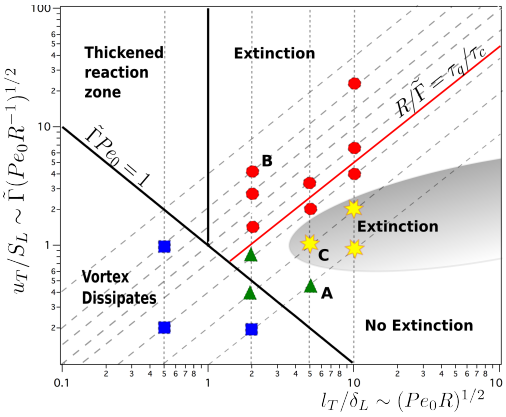


FIGURE 6. Spectral diagram for spray flame-vortex interaction: the symbols represent numerical simulations performed here. Squares represent the vortex dissipation regime, triangles the "no extinction", circles the extinction due to strain rate, stars are for extinction due to fuel depletion.

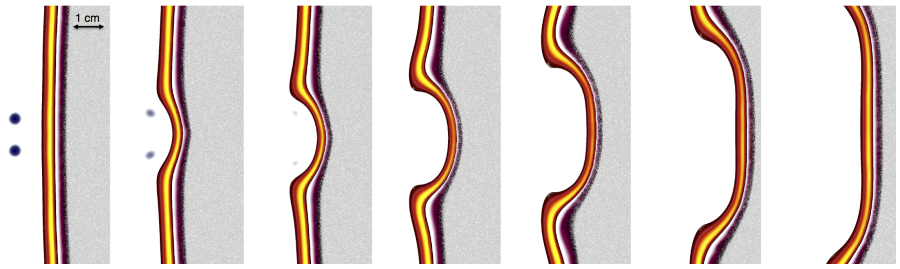


FIGURE 7. Temporal evolution of the spray flame-vortex interaction for the case without extinction (case A in Figure 6 corresponding to $r_v = 1.5e^{-3}$ $m$ and $A_\Gamma = 250$ $1/s$). OH isocontours (orange), vorticity contours (blue), droplet positions colored by droplet temperature (gray to black dots), gaseous fuel concentration (magenta).

Due to the engulfment of the flame in the wake of the vortices and the propagation of the flame front between the vortices, the reaction zone is finally reconnected. (iv) Extinction due to fuel depletion (case C, cf. Figure 9): this new region is observed for large values of $l_T/\delta_L$ and for velocity ratio $u_t/S_L$ becoming of order unity. This new regime was not observed by both the gaseous analysis and the spray spectral diagram. The competition between evaporation and mixing is changed as the vortices pass through the flame, resulting in a local fuel depletion, weakening the flame strength, and enhancing the extinction propensity.

Taking into account the evaporation time $\tau_v$ in the competition between mixing and chemistry seems to be sufficient to represent the strain rate extinction. However, this does not account for possible effects of a local lack of gaseous fuel that is the primary reason for extinction for spray flames, which does not occur in the classical gaseous flame-vortex configuration. The role of the evaporation is evident in Figure 9. Here, the interaction of the vortices with the flame and the droplet drives the flame to move toward the cold droplets, thereby consuming all droplets that were in the preheating region. The local

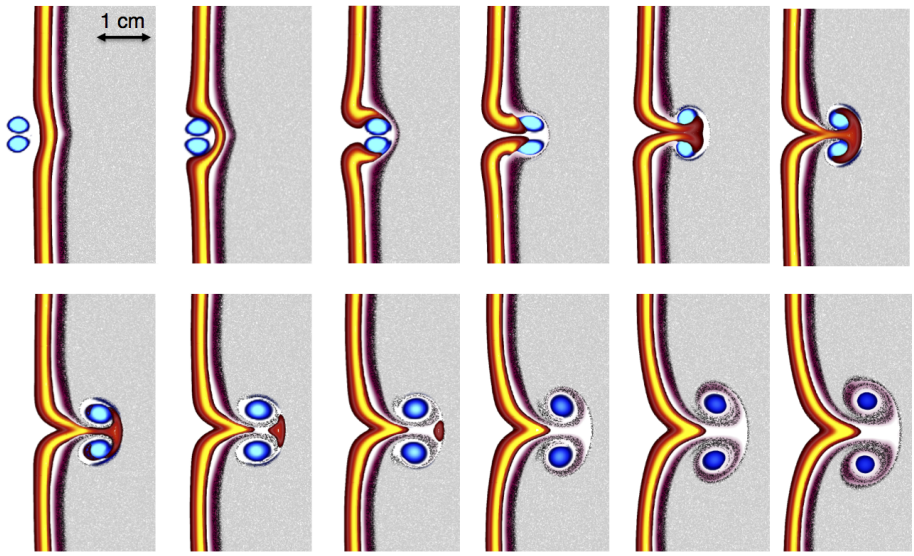


FIGURE 8. Temporal evolution of the spray flame-vortex interaction for the case with extinction due to strain rate (case B in Figure 6 corresponding to $r_v = 6.0e^{-4}$ $m$ and $A_\Gamma = 5000$ $1/s$). OH isocontours (orange), vorticity contours (blue), droplet positions colored by droplet temperature (gray to black dots), gaseous fuel concentration (magenta).

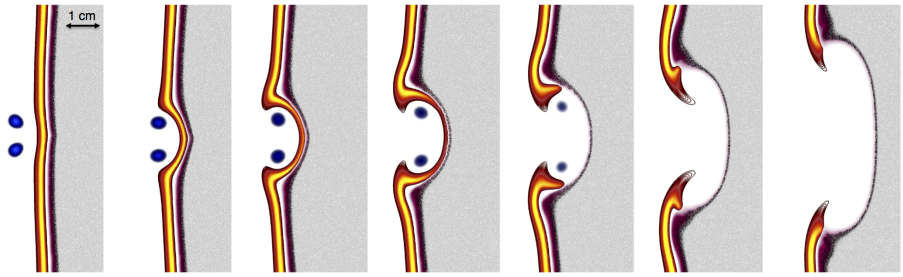


FIGURE 9. Temporal evolution of the spray flame-vortex interaction for the case of extinction due to fuel depletion (case C in Figure 6 corresponding to $r_v = 6.0e^{-4}$ $m$ and $A_\Gamma = 500$ $1/s$). OH isocontours (orange), vorticity contours (blue), droplet positions colored by droplet temperature (gray to black dots), gaseous fuel concentration (magenta).

fuel concentration is low since all fuel has been consumed by the flame passage and the droplets are too cold to evaporate. As such, the flame is no longer sustained by fuel supply, and consequently extinguishes. It worth to be mentioned that for the cases studied in this work, the extinction due to fuel depletion always leads to a global extinction of the flame. By contrast, extinction due to strain rate presents both a reignition or a global extinction depending on the operating conditions.

## 8. Conclusions

The spectral diagram suggested by Vera *et al.* (2007) for gaseous flame-vortex interactions was extended to spray flames. An analytical derivation was presented, based on the influence of the evaporation time on the quenching time of the flame. To confirm the spectral diagrams for gaseous and spray flames, numerical simulations were performed

by considering a two-dimensional counterflow configuration using a detailed chemistry description and a Lagrangian tracking for the droplets. Results demonstrate the validity of the gaseous spectral diagram. For the spray flames, the effect of the evaporation time on flame-vortex interaction was verified numerically. Moreover, the existence of a new extinction region was identified for small vortex velocities, which does not exist for gaseous flames and was not expected analytically for spray flames relying solely on the vaporization time.

## Acknowledgments

The authors gratefully acknowledge financial support through NASA with Award Nos. NNX14CM43P and NNM13AA11G and thank Prof. Heinz Pitsch for permission to use his code for this DNS-analysis. The resources of the National Energy Research Scientific Computing Center, which is supported by the Office of Science of the U.S. Department of Energy under Contract No. DE-AC02-05CH11231, are also acknowledged.

## REFERENCES

Ballal, D. R. & Lefebvre, A. H. 1981 Flame propagation in heterogeneous mixtures of fuel droplets, fuel vapor and air. In *Proc. Combust. Inst.* **18**, 321–327.

Dvorjetski, A. & Greenberg, J. 2002 Steady-state and extinction analyses of counterflow spray diffusion flames with arbitrary finite evaporation rate. *Combust. Sci. Tech.* **174**, 187–208.

Fernandez-Tarrazo, E., Sanchez, A., Linan, A. & Williams, F. 2006 A simple one-step chemistry model for partially premixed hydrocarbon combustion. *Combust. Flame* **147**, 32–38.

Hermanns, M., Vera, M. & Liñán, A. 2007 On the dynamics of flame edges in diffusion-flame/vortex interactions. *Combust. Flame* **149**, 32–48.

Lemaire, A., Meyer, T. R., Zähringer, K., Gord, J. R. & Rolon, J. C. 2002 PIV/PLIF investigation of two-phase vortex-flame interactions. *11th Int. Symp. on Applications of Laser Techniques to Fluid Mechanics* .

Lemaire, A., Zähringer, K., Meyer, T. R. & Rolon, J. C. 2005 Unsteady effects on flame extinction limits during gaseous and two-phase flame/vortex interactions. *Proc. Combust. Inst.* **30**, 475–483.

Mantel, T., Samaniego, J. M. & Bowman, C. T. 1999 Fundamental mechanisms in premixed turbulent flame propagation via vortex-flame interactions - part II: numerical simulation. *Combust. Flame* **118**, 557–582.

Miller, R. & Bellan, J. 1999 Direct numerical simulation of a confined three-dimensional gas mixing layer with one evaporating hydrocarbon-droplet-laden stream. *J. Fluid Mech.* **384**, 293–338.

Peters, N. 1984 Laminar diffusion flamelet models in non-premixed turbulent combustion. *Prog. Energy Comb. Sci.* **10**, 319 – 339.

Poinsot, T. & Veynante, D. 2012 *Theoretical and Numerical Combustion*, 3rd ed, R.T. Edwards.

Poinsot, T., Veynante, D. & Candel, S. 1991 Quenching processes and premixed turbulent combustion diagrams. *J. Fluid Mech.* **228**, 561–605.

Renard, P. H., Thévenin, D., Rolon, J. C. & Candel, S. 2000 Dynamics of flame/vortex interactions. *Prog. Energy Comb. Sci.* **26**, 225–282.

Réveillon, J. & Vervisch, L. 2005 Analysis of weakly turbulent diluted-spray flames and spray combustion regimes. *J. Fluid Mech.* **537**, 317–347.

Santoro, V. & Gomez, A. 2002 Extinction and reignition in counterflow spray diffusion flames interacting with laminar vortices. *Proc. Combust. Inst.* **29**, 585–592.

Santoro, V., Kyritsis, D. & Gomez, A. 2000 An experimental study of vortex-flame interaction in counterflow spray diffusion flames. *Proc. Combust. Inst.* **28**, 1023–1030.

Senoner, J. M. 2010 *Large eddy simulation of the two phase flow in an aeronautical burner using the Euler-Lagrange approach.* Ph.D. Thesis, INP Toulouse.

Shashank 2012 *High fidelity simulation of reactive liquid fuel jets.* Ph.D. Thesis, Stanford University.

Shiah, S.-M. & Sichel, M. 1993 On the interaction of a dense spray diffusion flame and a potential vortex. *AIAA paper 93-0901*.

Sirjean, B., Dames, E., Sheen, D. A. & Wang, H. 2009 Simplified chemical kinetic models for high-temperature oxidation of C1 to C12 n-alkanes. *6th US National Combustion Meeting* Paper 23F1.

Thevenin, D., Renard, P. H., Rolon, C. & Candel, S. 1998 Extinction processes during a non-premixed flame vortex interaction. In *27th Symp. (Int.) on Combustion*, pp. 719–726. The Combustion Institute, Pittsburgh.

Vera, M., Hermanns, M. & Liñán, A. 2007 A combustion diagram to characterize the regimes of interaction of non-premixed flames and strong vortices. In $3^{rd}$ *European Combustion Meeting*.

Vie, A., Franzelli, B., Gao, Y., Lu, T., Wang, H. & Ihme, M. 2014 Analysis of segregation and bifurcation in turbulent spray flames: A 3d counterflow configuration. *Proc. Combust. Inst.*, doi:10.1016/j.proci.2014.06.083.